

Stacked Intelligent Metasurfaces for Multiuser Downlink Beamforming in the Wave Domain

Jiancheng An, *Member, IEEE*, Marco Di Renzo, *Fellow, IEEE*,
 Mérouane Debbah, *Fellow, IEEE*, H. Vincent Poor, *Life Fellow, IEEE*,
 and Chau Yuen, *Fellow, IEEE*

Abstract

Intelligent metasurface has recently emerged as a promising technology that enables the customization of wireless environments by harnessing large numbers of inexpensive configurable scattering elements. However, prior studies have predominantly focused on single-layer metasurfaces, which have limitations in terms of the number of beam patterns they can steer accurately due to practical hardware restrictions. In contrast, this paper introduces a novel stacked intelligent metasurface (SIM) design. Specifically, we investigate the integration of SIM into the downlink of a multiuser multiple-input single-output (MISO) communication system, where a SIM, consisting of a multilayer metasurface structure, is deployed at the base station (BS) to facilitate transmit beamforming in the electromagnetic wave domain. This eliminates the need for conventional digital beamforming and high-resolution digital-to-analog converters at the BS. To this end, we formulate an optimization problem that aims to maximize

This research was supported in part by the Ministry of Education, Singapore, under its MOE Tier 2 (Award number MOE-T2EP50220-0019). Any opinions, findings and conclusions or recommendations expressed in this material are those of the author(s) and do not reflect the views of the Ministry of Education, Singapore. The work of M. Di Renzo was supported in part by the European Commission through the H2020 ARIADNE project under grant agreement number 871464 and through the H2020 RISE-6G project under grant agreement number 101017011, and by the Agence Nationale de la Recherche (ANR PEPR-5G and Future Networks, grant NF-PERSEUS, 22-PEFT-004). This article was presented in part at the IEEE International Conference on Communications (ICC), Rome, Italy, 2023 [1]. (*Corresponding author: Chau Yuen.*)

J. An and C. Yuen are with the School of Electrical and Electronics Engineering, Nanyang Technological University, Singapore 639798 (e-mail: jiancheng_an@163.com; chau.yuen@ntu.edu.sg).

M. Di Renzo is with Université Paris-Saclay, CNRS, CentraleSupélec, Laboratoire des Signaux et Systèmes, 91192 Gif-sur-Yvette, France (e-mail: marco.di-renzo@universite-paris-saclay.fr).

M. Debbah is with Khalifa University of Science and Technology, P O Box 127788, Abu Dhabi, UAE (email: merouane.debbah@ku.ac.ae).

H. Vincent Poor is with the Department of Electrical and Computer Engineering, Princeton University, Princeton, NJ 08544 USA (e-mail: poor@princeton.edu).

the sum rate of all user equipments by jointly optimizing the transmit power allocation at the BS and the wave-based beamforming at the SIM, subject to both the transmit power budget and discrete phase shift constraints. Furthermore, we propose a computationally efficient algorithm for solving this joint optimization problem and elaborate on the potential benefits of employing SIM in wireless networks. Finally, the numerical results corroborate the effectiveness of the proposed SIM-enabled wave-based beamforming design and evaluate the performance improvement achieved by the proposed algorithm compared to various benchmark schemes. It is demonstrated that considering the same number of transmit antennas, the proposed SIM-based system achieves about 200% improvement in terms of sum rate compared to conventional MISO systems.

Index Terms

Stacked intelligent metasurface (SIM), wave-based beamforming, power allocation, reconfigurable intelligent surface (RIS).

I. INTRODUCTION

In the past decade, various advanced wireless technologies such as millimeter-wave (mmWave) communications and massive multiple-input multiple-output (MIMO) systems have been developed to enhance network capacity and enable ubiquitous wireless connectivity [2]. Nonetheless, the practical implementation of these technologies is restricted by their prohibitive energy consumption and expensive hardware equipment [3]. In particular, mmWave communications are hindered by high atmospheric attenuation, thus generally demanding costly and energy-intensive transceivers [4]. Additionally, the substantial spatial multiplexing gain in massive MIMO systems may be compromised under extremely poor scattering conditions, even with a large number of active elements and excessive energy usage [5]. As a result, it has become clear that it is necessary for the future evolution of wireless networks to undergo a fundamental paradigm shift from solely increasing network capacity to prioritizing energy sustainability [6], [7].

Within this context, reconfigurable intelligent surface (RIS) has recently emerged as a disruptive technology that effectively improves both spectrum and energy efficiencies in wireless networks [8]–[13]. In general, an RIS is made of an artificial metasurface consisting of a large number of low-cost nearly passive elements. Each element can independently impose an ad-

justable phase shift on the incident electromagnetic (EM) waves [14]–[16]. By adjusting the phase shifts of all the elements with the aid of a smart controller (e.g., a field programmable gate array (FPGA)), the RIS is capable of manipulating the reflected and/or transmitted EM waves, thus creating favorable propagation environments appropriately shaping dynamic wireless channels [17]–[19]. Compared to conventional active MIMO relays, RISs operate in a nearly passive mode, eliminating self-interference issues and significantly reducing the energy consumption [14], [20]. Additionally, RIS can be easily integrated into existing cellular/WiFi networks without replacing the current hardware at the base stations (BS) and user equipment (UE) [9], [21]. Thanks to these outstanding features, RIS has attracted considerable research interest for enhancing the quality-of-service (QoS) performance of wireless networks in various typical communication scenarios [22]–[32].

To be more specific, Huang *et al.* [10] utilized an RIS to enhance the energy efficiency (EE) of downlink transmissions in multiuser multiple-input single-output (MISO) communications. They achieved a 300% improvement in EE compared to conventional amplify-and-forward relays by optimizing both the transmit power allocation and the phase shifts of RIS [10]. Following this, Wu and Zhang [18] studied the minimization of the transmit power by jointly optimizing the digital beamforming at the BS and the analog beamforming at the RIS, subject to a given set of QoS requirements at the UE receivers. Their analytical results demonstrated a 6 dB power gain by doubling the number of reflecting elements [14]. Furthermore, Guo *et al.* [26] examined the problem of maximizing the weighted sum rate in an RIS-aided multiuser MISO downlink communication system while accounting for imperfect channel state information (CSI). In order to reduce the excessive pilot signaling overhead required for probing a large number of reflected channels, phase shift optimization based on large-scale channel statistics was investigated in [32]. Motivated by this, An *et al.* [5], [11] proposed a codebook-based protocol that strikes favorable trade-offs among QoS, pilot overhead, and computational complexity.

Nevertheless, existing research efforts on RIS-assisted wireless networks, e.g., [14]–[30], [33], typically rely on a single-layer metasurface structure, which confines the available degrees-of-freedom (DoF) for adjusting the beam patterns. Furthermore, for the sake of reducing the implementation cost of RIS deployments, each reflecting element is restricted to have only a

TABLE I
A COMPARISON BETWEEN WAVE-BASED BEAMFORMING AND OTHER BEAMFORMING SCHEMES

Beamforming scheme	Hardware implementation	Computing speed	Hardware cost	Energy consumption	ADC/DAC resolution	Number of RF chains
Fully digital [34]	Baseband microprocessor	Slow	High	High	High	Large
Hybrid digital and analog [3]	Baseband microprocessor, and analog phase shifters	Moderate	Moderate	Moderate	Moderate	Moderate
Hybrid active and passive [18]	Baseband microprocessor, and single programmable metasurface	Fast	Low	Low	Moderate	Moderate
Proposed wave-based	Multiple programmable metasurfaces	Very fast	Very low	Very low	Low	Small

discrete number of phase shifts, inevitably leading to beam misalignment in the desired service area and impairing the anticipated performance gains [11], [18]. In addition, recent research progress has demonstrated that RISs lack the capability of individually suppressing the inter-user interference due to their intrinsic single-layer structure and practical hardware constraints on configuration network [26].

Motivated by these observations, we proposed a stacked intelligent metasurface (SIM) device in [1], [35]. By stacking an array of programmable metasurfaces, a SIM has a structure similar to artificial neural networks (ANN), thus having remarkable signal processing capabilities compared to its single-layer counterpart, e.g., an RIS. Most remarkably, the forward propagation in SIM is completed at the speed of light, which is in contrast to conventional ANNs whose computational speed depends on that of existing commercial microprocessors. It is important to note that the proposed SIM is firmly grounded on the latest technological advances in wave-based computing and tangible hardware prototypes [36], [37], and it is not a pure mathematical abstraction. To be more specific, Lin *et al.* [36] developed a diffractive deep neural network (D²NN) employing three-dimensional (3D) printed optical lenses. Such a 3D printed D²NN takes advantage of the wave properties of photons, allowing for parallel calculations at the speed of light [36]. Once fabricated, however, its interconnection structure becomes fixed and cannot be retrained for other tasks. To overcome this limitation, Liu *et al.* [37] designed a programmable D²NN based on a SIM-like device, where each meta-atom acts as a reprogrammable artificial neuron. They demonstrated that this programmable D²NN is capable of executing various complex signal

processing and computational tasks, such as image classification, by flexibly manipulating the EM waves propagating through its multiple layers [37].

Based on these experimental results, we proposed a SIM-based transceiver design for point-to-point MIMO communication systems [35]. Different from conventional MIMO designs, SIM is able to automatically accomplish precoding and combining as the EM waves propagate through it. As a result, each data stream can be radiated and recovered independently at the corresponding transmit and receive ports. When considering practical digital baseband modulation techniques, only low-resolution analog-to-digital converters (ADCs) and digital-to-analog converters (DACs) are required without compromising the error performance. This is in contrast to the utilization of low-resolution ADCs/DACs in massive MIMO systems, which typically results in a non-negligible performance penalty [38]. Furthermore, a SIM-enabled transceiver design for multiuser MISO downlink communication systems was developed in [1]. Therein, a SIM was integrated with the BS to perform transmit beamforming directly in the EM domain. This novel paradigm eliminates the need for digital beamforming and operates with a moderate number of radio frequency (RF) chains, which significantly reduces the hardware cost and energy consumption, while substantially decreasing the precoding delay thanks to the processing performed in the wave domain [35].

Nevertheless, our previous works in [1], [35] assume that the meta-atoms of the SIM can apply any tuning coefficient (continuous tuning), which may be difficult to achieve in practice. Given this, this paper extends the SIM-based transceiver in [1] by considering meta-atoms that can only be tuned discretely. Specifically, we focus on a multiuser MISO downlink communication system and incorporate a SIM at the BS to directly perform downlink multiuser beamforming in the EM wave domain. Before proceeding further, we explicitly contrast the proposed SIM-enabled wave-based beamforming scheme with the conventional counterparts including fully digital beamforming [34], hybrid digital and analog beamforming [3], as well as hybrid active and passive beamforming [18] in Table I. More specifically, the main contributions of this paper are summarized as follows:

- First, we present a SIM-based transceiver designed for the downlink of a multiuser MISO wireless system. In particular, a SIM is deployed to enhance the downlink communication

from a multiple-antenna BS to multiple single-antenna UEs. Thanks to the remarkable signal processing capabilities offered by the multilayer metasurface structure, the SIM allows for transmit beamforming in the EM wave domain. As a result, the conventional digital beamforming schemes and high-resolution DACs are completely eliminated from the BS.

- Then, we formulate an optimization problem aiming at maximizing the sum rate of all UEs via jointly optimizing the transmit power allocation at the BS and the wave-based beamforming at the SIM, subject to both a total transmit power budget and the implementation of discrete phase shifts. The formulated joint optimization problem, however, turns out to be a mixed integer non-linear programming (MINLP) problem, where the transmit power allocation coefficients and the discrete phase shifts are deeply coupled within the non-convex objective function, rendering it challenging to obtain the optimal solution.
- To tackle this challenge, we propose a computationally efficient alternating optimization algorithm by decomposing the joint power allocation and wave-based beamforming optimization problem into two nested subproblems. The first subproblem deals with the conventional power allocation for multiuser interference channels, which can be effectively solved by modifying the iterative water-filling algorithm. The second subproblem involves optimizing the phase shifts of the SIM. To address this, we propose a pair of suboptimal algorithms including the projected gradient ascent algorithm and the successive refinement method.
- We further provide useful insights into the potential benefits of employing SIM-based transceivers. Finally, we illustrate numerical results to evaluate the efficacy of the wave-based beamforming scheme, taking into account the practical constraint of discrete phase shifts. Specifically, it is demonstrated that the proposed SIM-based transceiver is capable of efficiently carrying out the transmit beamforming within a few nanoseconds. Moreover, we substantiate the enhanced performance of the proposed alternating optimization algorithm in comparison to various benchmark schemes.

The rest of this paper is structured as follows. Firstly, Section II introduces the system model of a SIM-assisted multiuser downlink MISO wireless system. Then, Section III-A formulates the joint power allocation and wave-based beamforming problem. In order to solve this challenging

problem, we propose an alternating optimization algorithm in Section III-B. Furthermore, Section IV provides numerical results that evaluate the performance of the proposed wave-based beamforming scheme. Finally, Section V concludes the paper.

Notations: Scalars are denoted by italic letters; column vectors and matrices are represented by boldface lower-case and upper-case symbols, respectively; j is the imaginary unit satisfying $j^2 = -1$. Moreover, $|z|$, $\Re(z)$, and $\Im(z)$ denote the absolute value, real part, and imaginary part, respectively, of a complex number z ; $(\cdot)^T$ and $(\cdot)^H$ denote the transpose and Hermitian transpose, respectively; $\text{diag}(x_1, x_2, \dots, x_N)$ generates a diagonal matrix with x_1, x_2, \dots, x_N being its diagonal entries; $\mathbf{0}$ denotes the all-zero vector of appropriate dimension, while \mathbf{I}_N represents the $N \times N$ identity matrix; $\mathbb{C}^{x \times y}$ represents the space of $x \times y$ complex-valued matrices. Furthermore, $\lfloor \cdot \rfloor$, $\lceil \cdot \rceil$, $\lceil \cdot \rceil$, and $\text{mod}(\cdot)$ represent the floor, rounding, ceiling, and modulo operator, respectively, while $\log_a(\cdot)$ is the logarithmic function with base a ; $\frac{\partial f}{\partial x}$ denotes the partial derivative of a function f with respect to x . The distribution of a circularly symmetric complex Gaussian random vector with a mean vector \mathbf{v} and a covariance matrix Σ is expressed as $\sim \mathcal{CN}(\mathbf{v}, \Sigma)$, where \sim stands for “distributed as”; $\text{sinc}(x) = \frac{\sin(\pi x)}{\pi x}$ is the normalized sinc function.

II. SYSTEM MODEL

As shown in Fig. 1, we consider the downlink of a multiuser MISO wireless system, where a SIM is deployed to assist the communication from a BS equipped with M antennas to K single-antenna UEs within a given frequency band. In particular, the SIM is fabricated by utilizing an array of L metasurfaces, each consisting of N meta-atoms¹. Moreover, the SIM is connected to a smart controller, such as a customized FPGA, which is capable of independently adjusting the phase shift of the EM waves transmitted through each meta-atom [11], [18]. Accordingly, the forward propagation process in SIM resembles a fully connected ANN. By properly training the interconnection architecture, the SIM can directly perform the downlink beamforming in the EM wave domain [37]. Let $\mathcal{L} = \{1, 2, \dots, L\}$, $\mathcal{N} = \{1, 2, \dots, N\}$, and $\mathcal{K} = \{1, 2, \dots, K\}$ denote the sets of metasurfaces, meta-atoms on each metasurface layer, and UEs, respectively.

¹We assume an identical number of meta-atoms on each metasurface just for the sake of simplicity but not loss of generality.

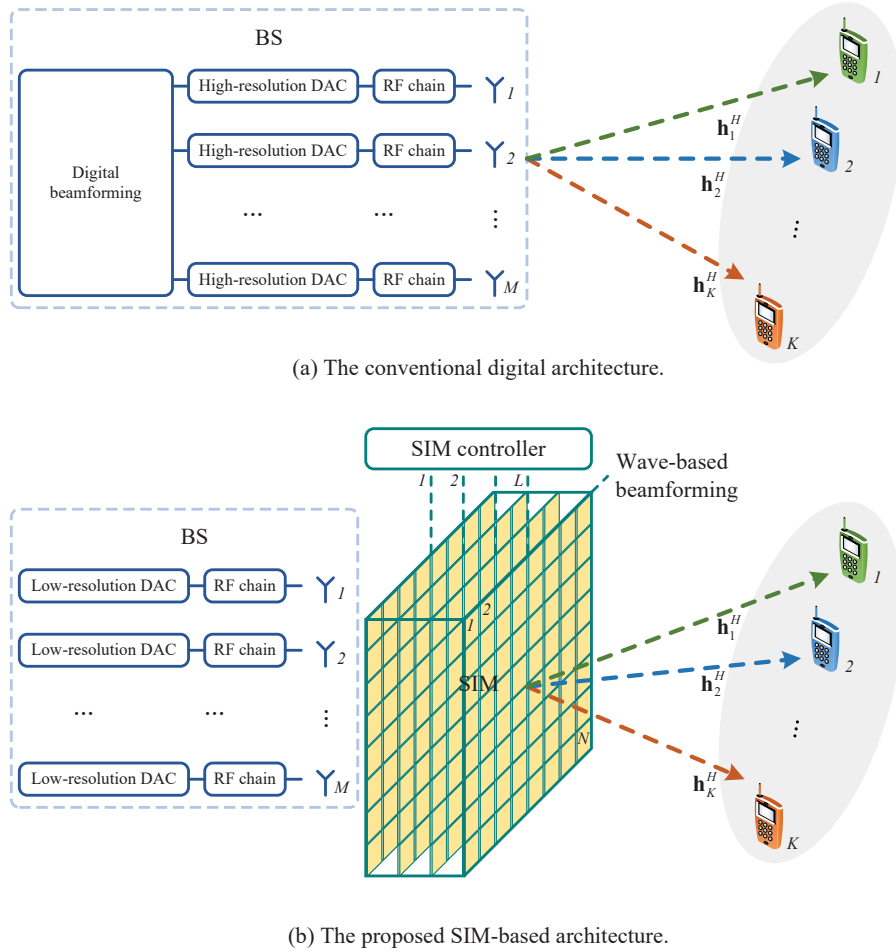


Fig. 1. A contrast of SIM-based and conventional multiuser MISO wireless systems.

Specifically, the complex-valued gain of the n -th meta-atom on the l -th metasurface layer is represented by $\alpha_n^l e^{j\theta_n^l}$, $\forall n \in \mathcal{N}$, $\forall l \in \mathcal{L}$, where $\alpha_n^l \in [0, 1]$ and $\theta_n^l \in [0, 2\pi)$ are the corresponding amplitude and phase shift, respectively. In order to achieve higher energy efficiency, each meta-atom is generally designed to maximize the signal transmission [5], [10]. As such, we assume $\alpha_n^l = 1$, $\forall n \in \mathcal{N}$, $\forall l \in \mathcal{L}$ throughout this paper. Additionally, in practical implementations, the phase shift of each meta-atom is limited to a finite number of discrete values. For simplicity, we assume that the discrete phase shift set \mathcal{B} is obtained by uniformly quantizing the interval $[0, 2\pi)$ into 2^b levels, with b representing the number of control bits. Thus, the set of legitimate phase shift values for each meta-atom is given by

$$\mathcal{B} = \{0, \Delta_\theta, 2\Delta_\theta, \dots, (2^b - 1) \Delta_\theta\}, \quad (1)$$

where $\Delta_\theta = 2\pi/2^b$ represents the phase shift resolution. As a result, the diagonal phase shift matrix Φ^l of the l -th metasurface layer can be written as

$$\Phi^l = \text{diag} \left(e^{j\theta_1^l}, e^{j\theta_2^l}, \dots, e^{j\theta_N^l} \right) \in \mathbb{C}^{N \times N}, \quad \forall l \in \mathcal{L}, \quad (2)$$

where $\theta_n^l \in \mathcal{B}$, $\forall n \in \mathcal{N}$, $\forall l \in \mathcal{L}$.

Furthermore, let $\mathbf{W}^l \in \mathbb{C}^{N \times N}$, $\forall l \neq 1$, $l \in \mathcal{L}$ represent the transmission matrix from the $(l-1)$ -st to the l -th metasurface layer and $\mathbf{w}_m^1 \in \mathbb{C}^{N \times 1}$ denote the transmission vector from the m -th transmit antenna to the first metasurface layer of the SIM. According to the Rayleigh-Sommerfeld diffraction theory [36], [37], [39], the (n, n') -th entry $w_{n,n'}^l$ of \mathbf{W}^l is given by

$$w_{n,n'}^l = \frac{d_x d_y \cos \chi_{n,n'}^l}{d_{n,n'}^l} \left(\frac{1}{2\pi d_{n,n'}^l} - j \frac{1}{\lambda} \right) e^{j2\pi d_{n,n'}^l / \lambda}, \quad (3)$$

for $\forall l \in \mathcal{L}$, where λ is the wavelength, $d_{n,n'}^l$ denotes the transmission distance of the corresponding link, $\chi_{n,n'}^l$ represents the angle between the propagation direction and the normal direction of the $(l-1)$ -st metasurface layer, while $d_x \times d_y$ characterizes the size of each meta-atom. Similarly, the n -th entry $w_{n,m}^1$ of \mathbf{w}_m^1 can be obtained using (3).

According to the Huygens–Fresnel principle [36], the EM wave passing through each meta-atom on the previous metasurface layer will act as a point source and will illuminate all the meta-atoms on the subsequent metasurface layer. Furthermore, all EM waves impinging on a meta-atom of the current metasurface layer are superimposed and then act as the incident wave onto this meta-atom. As such, the forward propagation in the SIM can be expressed as

$$\mathbf{G} = \Phi^L \mathbf{W}^L \Phi^{L-1} \dots \Phi^2 \mathbf{W}^2 \Phi^1 \in \mathbb{C}^{N \times N}. \quad (4)$$

In practical implementations, a SIM is typically housed within a metallic support structure that is coated with wave-absorbing material [37]. Hence, any diffraction effects between non-adjacent metasurfaces can be considered negligible and are disregarded in (4).

In this paper, we consider a quasi-static flat-fading model for all channels illustrated in Fig. 1. Specifically, let $\mathbf{h}_k^H \in \mathbb{C}^{1 \times N}$, $\forall k \in \mathcal{K}$ denote the baseband equivalent channel from the last metasurface layer to the k -th UE, which is modeled according to a correlated Rayleigh fading

distribution [40]–[42], as follows:

$$\mathbf{h}_k \sim \mathcal{CN}(\mathbf{0}, \beta_k \mathbf{R}), \quad \forall k \in \mathcal{K}, \quad (5)$$

where β_k represents the distance-dependent path loss of the link between the SIM and UE k , while $\mathbf{R} \in \mathbb{C}^{N \times N}$ is a positive semidefinite matrix that characterizes the spatial correlation among the channels associated with different meta-atoms on the last layer. Assuming an isotropic scattering environment with uniformly distributed multipath components, the (n, n') -th entry of \mathbf{R} can be expressed as [43]

$$\mathbf{R}_{n,n'} = \text{sinc}\left(\frac{2d_{n,n'}}{\lambda}\right), \quad (6)$$

where $d_{n,n'}$ represents the corresponding meta-atom spacing.

Next, we consider the downlink data transmission. Note that in sharp contrast to the conventional digital precoding that assigns each symbol an individual beamforming vector, we perform wave-based beamforming with the aid of a SIM. As a result, each data stream is transmitted directly from the corresponding antenna at the BS, which implies that the BS needs to select a set of K appropriate antennas from the total of M antennas in advance. This antenna selection process resembles that in conventional MIMO systems with a limited number of RF chains at the BS [44], [45]. Since this paper focuses on wave-based beamforming, we assume that $M = K$ for the sake of simplicity. The joint antenna selection and wave-based beamforming design are reserved for future study.

Specifically, we denote the information-bearing symbol to the k -th UE as s_k , $\forall k \in \mathcal{K}$, which is modeled by an independent and identically distributed (i.i.d.) sequence of random variables with zero means and unit variances. Let $p_k \geq 0$ represent the power allocated to the k -th UE. Accordingly, the total transmit power constraint at the BS can be expressed as

$$\sum_{k=1}^K p_k \leq P_T, \quad (7)$$

where P_T represents the transmit power budget at the BS. Furthermore, upon superimposing all the signals propagating through the SIM, the composite signal r_k received at the k -th UE is

given by

$$r_k = \mathbf{h}_k^H \mathbf{G} \sum_{k'=1}^K \mathbf{w}_{k'}^1 \sqrt{p_{k'}} s_{k'} + n_k, \quad \forall k \in \mathcal{K}, \quad (8)$$

where $n_k \sim \mathcal{CN}(0, \sigma_k^2)$ denotes the additive white Gaussian noise (AWGN) with σ_k^2 representing the average noise power at the receiver of UE k .

By treating the signal components of the remaining $(K - 1)$ UEs as interference, the signal-to-interference-plus-noise-ratio (SINR) at the receiver of UE k can be expressed as

$$\gamma_k = \frac{|\mathbf{h}_k^H \mathbf{G} \mathbf{w}_k^1|^2 p_k}{\sum_{k' \neq k} |\mathbf{h}_k^H \mathbf{G} \mathbf{w}_{k'}^1|^2 p_{k'} + \sigma_k^2}, \quad \forall k \in \mathcal{K}. \quad (9)$$

As a result, the sum rate of these K UEs is given by

$$R = \sum_{k=1}^K \log_2 (1 + \gamma_k). \quad (10)$$

Remark 1: Note that in (9), although UE k naively treats the signal components of the other UEs as interference while demodulating s_k , it is possible to optimize the phase shifts in \mathbf{G} to mitigate the inter-user interference, which constitutes the proposed “*wave-based beamforming*” design. While the wave-based beamforming scheme may appear to involve more matrix multiplication at first glance, it is important to highlight that all multiplications in (4) are automatically accomplished as the wave propagates through each metasurface layer. This new wave-based computing paradigm is fundamentally distinct from baseband digital beamforming.

Remark 2: By employing the time-division duplex (TDD) protocol, the BS can readily acquire the downlink CSI by leveraging channel reciprocity. It should be noted that the channel estimation in SIM-assisted wireless systems bears resemblance to that in the generalized spatial modulation scheme with a limited number of RF chains [46]. Evidently, all the channels associated with K UEs can be obtained by using at least $\lceil KN/M \rceil$ pilot symbols. Moreover, the phase shifts of SIM can be jointly designed with the uplink pilots to further enhance the channel estimation accuracy.

Remark 3: Due to practical hardware imperfections, such as the bending of metasurfaces, the

transmission coefficients $w_{n,n'}^l$ between adjacent metasurface layers may deviate from the values specified in (3). At the time of writing, there is no experimentally validated model available, which also leads to inevitable modeling errors in (3). Therefore, it is necessary to calibrate the transmission coefficients $w_{n,n'}^l$ before practical SIM deployment. This calibration process can be accomplished by measuring the signals received at some auxiliary probes and applying the well-known backpropagation algorithm [37].

III. JOINT POWER ALLOCATION AND WAVE-BASED BEAMFORMING: PROBLEM FORMULATION AND SOLUTION

A. Problem Formulation

In this paper, we aim to maximize the sum rate of all UEs by jointly optimizing the transmit power allocation at the BS and the wave-based beamforming at the SIM, subject to the total transmit power budget and the discrete phase shift constraints. To characterize the ultimate performance limit, we assume that the CSI of all the channels in Fig. 1 is perfectly known by the BS. By introducing the variables $\mathbf{p} \triangleq [p_1, p_2, \dots, p_K]^T \in \mathbb{C}^{K \times 1}$, $\boldsymbol{\theta}^l \triangleq [\theta_1^l, \theta_2^l, \dots, \theta_N^l]^T \in \mathbb{C}^{N \times 1}$, and $\boldsymbol{\vartheta} \triangleq \{\boldsymbol{\theta}^1, \boldsymbol{\theta}^2, \dots, \boldsymbol{\theta}^L\}$, the joint power allocation and wave-based beamforming optimization problem is formulated as

$$(\mathcal{P}_A) : \max_{\mathbf{p}, \boldsymbol{\vartheta}} R = \sum_{k=1}^K \log_2(1 + \gamma_k) \quad (11a)$$

$$\text{s.t. } \gamma_k = \frac{|\mathbf{h}_k^H \mathbf{G} \mathbf{w}_k^1|^2 p_k}{\sum_{k' \neq k} |\mathbf{h}_k^H \mathbf{G} \mathbf{w}_{k'}^1|^2 p_{k'} + \sigma_k^2}, \quad \forall k, \quad (11b)$$

$$\mathbf{G} = \boldsymbol{\Phi}^L \mathbf{W}^L \boldsymbol{\Phi}^{L-1} \dots \boldsymbol{\Phi}^2 \mathbf{W}^2 \boldsymbol{\Phi}^1, \quad (11c)$$

$$\boldsymbol{\Phi}^l = \text{diag} \left(e^{j\theta_1^l}, e^{j\theta_2^l}, \dots, e^{j\theta_N^l} \right), \quad \forall l, \quad (11d)$$

$$\theta_n^l \in \mathcal{B}, \quad \forall n \in \mathcal{N}, \quad \forall l \in \mathcal{L}, \quad (11e)$$

$$\sum_{k=1}^K p_k \leq P_T, \quad (11f)$$

$$p_k \geq 0, \quad \forall k \in \mathcal{K}. \quad (11g)$$

Despite the conciseness of problem (\mathcal{P}_A) , it is generally challenging to obtain an optimal solution for the joint power allocation and wave-based beamforming design, due to the fact that the

optimization variables \mathbf{p} and $\boldsymbol{\vartheta}$ are deeply coupled within the non-convex objective function (11a). In addition, the constraints in (11e) restrict the θ_n^l to take discrete values, thereby rendering problem (\mathcal{P}_A) an NP-hard MINLP. To address this, we propose an alternating optimization algorithm in Section III-B to obtain a suboptimal solution for problem (\mathcal{P}_A) .

B. The Proposed Alternating Optimization Algorithm

The alternating optimization algorithm decomposes the joint optimization problem (\mathcal{P}_A) into a pair of nested subproblems: one involving the conventional power allocation among K interference channels, and the other focusing on the phase shift optimization. In each subproblem, we update only one of the optimization variables, either \mathbf{p} or $\boldsymbol{\vartheta}$, while keeping the other one fixed at its updated value in the previous iteration.

1) *Optimizing the Power Allocation \mathbf{p} with Given $\boldsymbol{\vartheta}$* : For any given SIM phase shifts $\boldsymbol{\vartheta} = \{\boldsymbol{\theta}^1, \boldsymbol{\theta}^2, \dots, \boldsymbol{\theta}^L\}$, the wave-based beamforming matrix \mathbf{G} can be determined by utilizing (4). As such, problem (\mathcal{P}_A) is simplified to

$$(\mathcal{P}_B) : \max_{\mathbf{p}} R \quad (12a)$$

$$\text{s.t.} \quad (11b), (11f), (11g). \quad (12b)$$

Note that problem (\mathcal{P}_B) turns out to be the traditional power allocation problem among K interference channels with a total power budget, which can be efficiently solved by employing the iterative water-filling algorithm [47], [48].

To elaborate, once an initial power allocation (e.g., average power allocation) is chosen, the interference power perceived by each UE can be calculated accordingly. At each iteration, UE k treats the interference caused by all other UEs as background noise. By treating the K interference channels as their parallel equivalents, the optimal power allocation solution for maximizing the sum rate can be obtained by employing the well-known water-filling principle as [49]

$$p_k = \left(p_{\text{WF}} - \frac{\sum_{k' \neq k}^K |\mathbf{h}_k^H \mathbf{G} \mathbf{w}_{k'}^1|^2 p_{k'} + \sigma_k^2}{|\mathbf{h}_k^H \mathbf{G} \mathbf{w}_k^1|^2} \right)^+, \quad (13)$$

for $\forall k \in \mathcal{K}$, where we have $(x)^+ \triangleq \max\{0, x\}$, while the water-filling level p_{WF} is determined using the bisection method such that $\sum_{k=1}^K p_k = P_{\text{T}}$ is satisfied at each iteration.

Nevertheless, as the power allocated for all UEs are simultaneously updated at each iteration, the plain iterative water-filling algorithm in (13) may not be stable when $K > 2$ [47]. To address this issue, we modify the update process by introducing a damping term. Specifically, the updated power allocation solution \mathbf{p} at each iteration is a weighted combination of the previous power allocation solution and the new one generated by the iterative water-filling step. Let $\mathbf{p}^{(*)}$ represent the new power allocation solution obtained using (13). Hence, we have

$$\mathbf{p}^{(i)} = \frac{1}{K}\mathbf{p}^{(*)} + \frac{K-1}{K}\mathbf{p}^{(i-1)}, \quad (14)$$

where $\mathbf{p}^{(i-1)}$ and $\mathbf{p}^{(i)}$ represent the power allocation solution at the $(i-1)$ -st and the i -th iteration, respectively.

After repeatedly applying (13) and (14) multiple times, the sum rate R will gradually approach its maximum value. In *Theorem 3* of [48], Jindal *et al.* have proven that the modified iterative water-filling algorithm incorporating a damping term is guaranteed to converge to the sum rate capacity for arbitrary values of K . In Section IV, we will numerically validate the convergence of the modified iterative water-filling algorithm.

2) *Optimizing the SIM Phase Shifts ϑ with Given \mathbf{p}* : Given a tentative power allocation solution \mathbf{p} , we then focus on the phase shift optimization subproblem, which is formulated as

$$(\mathcal{P}_{\mathcal{C}}): \quad \max_{\vartheta} \quad R \quad (15a)$$

$$\text{s.t.} \quad (11b) - (11e). \quad (15b)$$

In general, the globally optimal phase shifts for problem $(\mathcal{P}_{\mathcal{C}})$ can only be obtained via exhaustively searching through all legitimate phase shift values. As a result, the total computational complexity is given by $\mathcal{O}[(4N+3)K^2B^{LN}]$, where $(4N+3)$ represents the number of real-valued multiplications required to compute $|\mathbf{h}_k^H \mathbf{G} \mathbf{w}_{k'}^1|^2 p_{k'}$ in (11b) for each pair $(k, k') \in \mathcal{K}^2$, bearing in mind that $\mathbf{G} \mathbf{w}_k^1 \in \mathbb{C}^{N \times 1}$ is known *a priori* for each $\theta_n^l \in \mathcal{B}$. Note that the computational complexity of the exhaustive search grows exponentially with the number of metasurface layers

L and that of meta-atoms N on each layer, which is prohibitive even for a medium-sized SIM. Next, we propose a pair of computationally efficient algorithms, namely the projected gradient ascent and the successive refinement methods, to solve problem (\mathcal{P}_C) .

i) Successive Refinement Method: The suboptimal successive refinement algorithm iteratively optimizes each of the LN phase shifts. Specifically, by fixing the remaining $(LN - 1)$ phase shifts, we can find the optimal solution for the n -th discrete phase shift θ_n^l on the l -th metasurface layer via a one-dimensional search over \mathcal{B} , i.e.,

$$\hat{\theta}_n^l = \arg \max_{\theta_n^l \in \mathcal{B}} R, \quad \forall n \in \mathcal{N}, \quad \forall l \in \mathcal{L}. \quad (16)$$

The proposed successive refinement algorithm is guaranteed to converge due to the following two reasons. Firstly, by successively updating the phase shifts of all meta-atoms based on (16), the objective function value of (\mathcal{P}_C) in (15a) is non-decreasing as the iteration progresses [22]. Secondly, the optimal objective value of (\mathcal{P}_C) is upper-bounded as

$$R \stackrel{(a)}{\leq} \sum_{k=1}^K \log_2 \left(1 + \max_{\boldsymbol{\vartheta}} |\mathbf{h}_k^H \mathbf{G} \mathbf{w}_k^1|^2 \frac{P_k}{\sigma_k^2} \right), \quad (17)$$

where (a) holds due to the limited number of discrete phase shift values with restricted amplitude. With the converged discrete phase shifts, the maximum sum rate R can be obtained accordingly.

ii) Projected Gradient Ascent Method: Given that the optimization problem (\mathcal{P}_C) is a constrained maximization problem, we can employ the projected gradient ascent algorithm to iteratively update the phase shifts $\boldsymbol{\vartheta}$ until converging to the vicinity of a stationary point. The specific steps of the projected gradient ascent algorithm are outlined as follows:

Step 1: Initialize all phase shifts $\theta_n^l, \forall n \in \mathcal{N}, \forall l \in \mathcal{L}$ by discretizing the uniform random distribution into \mathcal{B} . Then, calculate the sum rate R by applying (10).

Step 2: Furthermore, compute the partial derivative values of R with respect to all the θ_n^l 's according to Proposition 1.

Proposition 1: For $\forall n \in \mathcal{N}, \forall l \in \mathcal{L}$, the partial derivative of R with respect to θ_n^l can be

obtained by

$$\frac{\partial R}{\partial \theta_n^l} = 2 \log_2 e \sum_{k=1}^K \delta_k \left(p_k \eta_{n,k,k}^l - \gamma_k \sum_{k' \neq k}^K p_{k'} \eta_{n,k,k'}^l \right), \quad (18)$$

where δ_k and $\eta_{n,k,k'}^l$ are defined by

$$\delta_k \triangleq \frac{1}{\sum_{k'=1}^K |\mathbf{h}_k^H \mathbf{G} \mathbf{w}_{k'}^1|^2 p_{k'} + \sigma_k^2}, \quad (19)$$

$$\eta_{n,k,k'}^l \triangleq \Im \left[e^{-j\theta_n^l} (\mathbf{w}_{k'}^1)^H \mathbf{u}_n^l (\mathbf{v}_n^l)^H \mathbf{h}_k \mathbf{h}_k^H \mathbf{G} \mathbf{w}_{k'}^1 \right], \quad (20)$$

respectively. Moreover, $(\mathbf{u}_n^l)^H$ and \mathbf{v}_n^l represent the n -th row of $\mathbf{U}^l \in \mathbb{C}^{N \times N}$ and the n -th column of $\mathbf{V}^l \in \mathbb{C}^{N \times N}$, which are defined by

$$\mathbf{U}^l \triangleq \begin{cases} \mathbf{W}^l \Phi^{l-1} \dots \Phi^2 \mathbf{W}^2 \Phi^1, & \text{if } l \neq 1, \\ \mathbf{I}_N, & \text{if } l = 1, \end{cases} \quad (21)$$

$$\mathbf{V}^l \triangleq \begin{cases} \Phi^L \mathbf{W}^L \Phi^{L-1} \dots \Phi^{l+1} \mathbf{W}^{l+1}, & \text{if } l \neq L, \\ \mathbf{I}_N, & \text{if } l = L, \end{cases} \quad (22)$$

respectively.

Proof: Please refer to Appendix A. ■

Step 3: After calculating all the partial derivatives of R with respect to θ_n^l based on (18), we proceed to simultaneously update all the phase shifts θ_n^l by

$$\theta_n^l \leftarrow \theta_n^l + \mu \frac{\partial R}{\partial \theta_n^l}, \quad \forall n \in \mathcal{N}, \quad \forall l \in \mathcal{L}, \quad (23)$$

where $\mu > 0$ is the *Armijo* step size, which is determined by leveraging the backtracking line search at each iteration [30].

Step 4: Since the phase shift vector updated by (23) may not be a feasible solution due to the discrete constraints in (11e), we then perform a restraining step to quantize θ_n^l into its nearest value in \mathcal{B} , i.e.,

$$\theta_n^l \leftarrow \arg \min_{\theta \in \mathcal{B}} |\theta - \theta_n^l|$$

Algorithm 1 The Alternating Optimization Algorithm for Joint Power Allocation and Wave-Based Beamforming.

- 1: **Input:** $\{\mathbf{W}^l\}_{l=1}^L$, $\{\mathbf{h}_k^H\}_{k=1}^K$, P_T , and \mathcal{B} .
 - 2: Initialize \mathbf{p} and ϑ that fulfill (11e) - (11g).
 - 3: **Repeat**
 - 4: Update \mathbf{p} by employing the modified iterative water-filling algorithm.
 - 5: Update ϑ by employing the projected gradient ascent or successive refinement method.
 - 6: **Until** The sum rate R in (10) achieves convergence.
 - 7: **Output:** \mathbf{p} and ϑ .
-

$$= \Delta_\theta \lceil \theta_n^l / \Delta_\theta \rceil, \quad \forall n \in \mathcal{N}, \quad \forall l \in \mathcal{L}, \quad (24)$$

bearing in mind that we have $\Delta_\theta = 2\pi/2^b$.

Step 5: Repeat **Steps 2** ~ **4** in a loop until the fractional increase of the sum rate becomes smaller than a preset threshold. Then, return the corresponding $\theta_n^l, \forall n \in \mathcal{N}, \forall l \in \mathcal{L}$ as the optimized phase shifts of the SIM.

The convergence of the projected gradient ascent algorithm to a local maximum can be guaranteed due to the fact that: *i*) the sum rate R is upper bounded by (17) and *ii*) the sum rate R is non-decreasing by choosing an appropriate *Armijo* step size μ at each iteration [50]. Nevertheless, since the quantization process at each iteration might impact the performance, we employ multiple initializations to enhance the reliability of the projected gradient ascent algorithm.

As a result, a suboptimal solution for (\mathcal{P}_A) can be achieved by iteratively carrying out the optimization procedures outlined in Section III-B. More explicitly, the overall alternating optimization algorithm solving problem (\mathcal{P}_A) is summarized in Algorithm 1.

C. Computational Complexity Analysis

The proposed alternating optimization algorithm is a nested iterative optimization process. Specifically, the outer loop tackles two subproblems for optimizing \mathbf{p} and ϑ , respectively, and each subproblem requires its own iterative updating method to find a solution. For the power allocation, in particular, the complexity of the iterative water-filling algorithm in Section III-B is $\mathcal{O}[K^2 I_{\text{IWF}}(4N + 3)]$, where I_{IWF} denotes the number of iterations required for achieving conver-

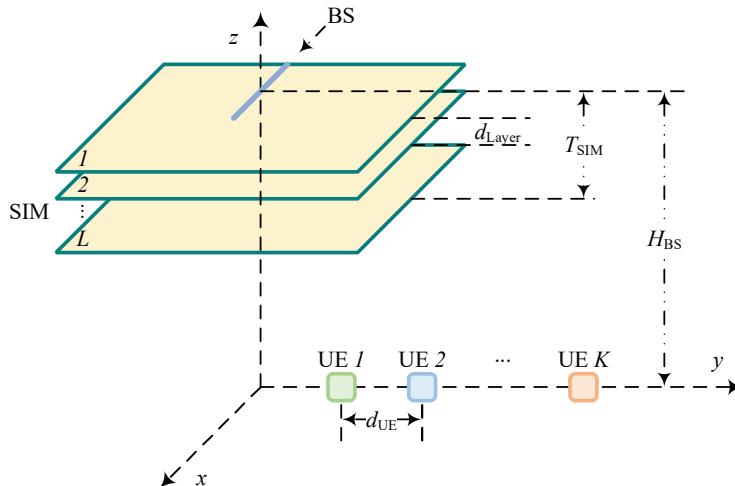


Fig. 2. Simulation setup of the considered SIM-assisted multiuser downlink MISO system.

gence. For the phase shift optimization, the complexity of the successive refinement algorithm to determine the phase shifts of SIM is given by $\mathcal{O}[K^2 L N B I_{\text{SR}} (4N + 3)]$, where I_{SR} represents the number of iterations required for achieving convergence of the successive refinement algorithm. Since the discrete phase shift set \mathcal{B} is typically small in practice, the successive refinement relying on one-dimensional search in (16) is computationally efficient. Furthermore, the gradient ascent algorithm has a computational complexity of $\mathcal{O}[2K^2 L N I_{\text{GA}} (4N + 3)]$, where the complexities of calculating (10), (18), and (20) are $\mathcal{O}[K^2 (4N + 3)]$, $\mathcal{O}(K^2)$, and $\mathcal{O}[K^2 (4N + 2)]$, respectively. Note that the complexity of the gradient ascent algorithm is independent of the cardinality of the discrete phase shift set \mathcal{B} , making it more efficient for the case with high-resolution meta-atoms. As a result, the total complexity of the alternating optimization approach can be expressed as $\mathcal{O}[I_{\text{AO}} K^2 (I_{\text{WF}} + L N \min(B I_{\text{SR}}, 2 I_{\text{GA}})) (4N + 3)]$, where I_{AO} denotes the number of iterations for the outer loop.

IV. NUMERICAL RESULTS

In this section, we provide numerical results to validate the effectiveness of the wave-based beamforming design and evaluate the sum rate of a SIM-assisted multiuser downlink MISO system utilizing the proposed algorithms.

A. Simulation Setups

As illustrated in Fig. 2, we examine the downlink of a SIM-assisted multiuser MISO system, where a BS is equipped with a uniform linear array (ULA) consisting of M antennas positioned along the x-axis. Furthermore, a SIM stacking multiple metasurfaces is integrated with the BS to perform the transmit beamforming in the EM wave domain. Each metasurface comprises a uniform planar array (UPA) parallel to the x-y plane. The center antenna/meta-atom of both the BS and metasurfaces align with the z-axis. The height of the BS is set to $H_{\text{BS}} = 10$ m, while the SIM has a thickness of $T_{\text{SIM}} = 5\lambda$. Hence, the spacing between adjacent metasurfaces in an L -layer SIM is $d_{\text{Layer}} = T_{\text{SIM}}/L$. Moreover, we assume that all metasurfaces are isomorphic, with N_x and N_y representing the number of meta-atoms along the x-axis and the y-axis, respectively. Thus, we have $N = N_x N_y$. For the sake of simplicity, we consider square metasurfaces with $N_x = N_y$. Furthermore, we assume a half-wavelength spacing between adjacent antennas/meta-atoms for both the BS and metasurfaces. The size of each meta-atom is $d_x = d_y = \lambda/2$. To mitigate the effects caused by the statistical positions of the UEs, we assume that K single-antenna UEs are uniformly distributed along a line originating from the reference point with a spacing of $d_{\text{UE}} = 10$ m, as shown in Fig. 2. Additionally, each antenna at the BS is assumed to have an antenna gain of 5 dBi, while each UE is equipped with a single antenna with 0 dBi gain [30].

Furthermore, the spatial attenuation coefficients $w_{n,n'}^l$ between neighboring metasurface layers in SIM and that from the transmit antenna array to the first metasurface layer are determined by (3). Specifically, the distance between the n' -th meta-atom of the $(l-1)$ -st metasurface and the n -th meta-atom of the l -th metasurface is given by $d_{n,n'}^l = \sqrt{d_{\text{Layer}}^2 + d_{n,n'}^2}$, where $d_{n,n'}$ is defined as follows:

$$d_{n,n'} = \frac{\lambda}{2} \sqrt{[|n - n'|/N_x]^2 + [\text{mod}(|n - n'|, N_x)]^2}. \quad (25)$$

In particular, the transmission distance between the m -th antenna and the n -th meta-atom on the first metasurface layer is determined by (26), as shown at the top of this page. Furthermore, we have $\cos \chi_{n,n'}^l = d_{\text{Layer}}/d_{n,n'}^l$ for $\forall l \in \mathcal{L}$. We assume a correlated Rayleigh fading channel

$$d_{n,m}^1 = \sqrt{d_{\text{Layer}}^2 + \left[\left(\text{mod}(n-1, N_x) - \frac{N_x-1}{2} \right) \frac{\lambda}{2} - \left(m - \frac{M+1}{2} \right) \frac{\lambda}{2} \right]^2 + \left(\lceil n/N_x \rceil - \frac{N_y+1}{2} \right)^2 \frac{\lambda^2}{4}}. \quad (26)$$

.....

model, i.e., (5), for all the wireless channels, while the spatial correlation matrix is determined by (6). The distance-dependent path loss is modeled as

$$\beta_k = C_0 (d_k/d_0)^{-\bar{n}}, \quad d_k \geq d_0, \quad (27)$$

where $d_k = \sqrt{(H_{\text{BS}} - T_{\text{SIM}})^2 + [d_{\text{UE}}(k-1)]^2}$ represents the link distance from the SIM to the k -th UE, while $C_0 = (\lambda/4\pi d_0)^2$ is the free space path loss at the reference distance of $d_0 = 1$ m [4], and the path loss exponent \bar{n} is set to $\bar{n} = 3.5$. Additionally, we consider a system operating at a carrier frequency of 28 GHz with a transmission bandwidth of 10 MHz and the effective noise power spectral density of -174 dBm/Hz for all UEs. Thus, we have $C_0 = -40$ dB and $\sigma_k^2 = -104$ dBm for $\forall k \in \mathcal{K}$.

Next, we evaluate the performance of the proposed algorithms in comparison to the four benchmark approaches outlined below:

- *Continuous phase shift:* We solve problem (\mathcal{P}_A) by relaxing all discrete optimization variables θ_n^l 's to their continuous counterparts. To solve the subproblem (\mathcal{P}_C) , we adapt the projected gradient ascent method by excluding **Step 4**;
- *Quantization scheme:* We directly quantize each of the continuous phase shifts obtained to its nearest discrete value in \mathcal{B} ;
- *Average power allocation:* We solve problem (\mathcal{P}_C) given the average power allocation solution;
- *Codebook method:* We randomly generate a phase shift vector codebook of size Q . For each phase shift in the codebook, we apply the iterative water-filling power allocation. Subsequently, the phase shift that yields the maximum sum rate is selected to finalize the SIM configuration.

Moreover, the threshold for terminating the iterations in the AO algorithm and the iterative

water-filling is set to 10^{-6} , while the maximum number of iterations in the AO algorithm, the inner iteration of the iterative water-filing and the backtracking line search is limited to 100. All simulation results are obtained by averaging over 1,000 channel realizations, each with independent small-scale fading. The codebook size is set to $Q = 10LN$ in our simulations.

B. Sum Rate Performance Evaluation of the Proposed Wave-Based Beamforming Design

First of all, Fig. 3a illustrates the sum rate R versus the number of metasurface layers L , where we set $N = 49$, $M = K = 4$, and $P_T = 10$ dBm. In particular, we consider $b = 2$ for the discrete phase shifts. By gradually increasing the number of metasurface layers from $L = 1$ to $L = 10$, we observe that the sum rate of the SIM-aided MISO system utilizing the optimized power allocation and wave-based beamforming improves, thanks to the ability of SIM to mitigate the inter-user interference in the EM wave domain. In addition, the sum rate exhibits a tendency to converge and achieves its peak at $L = 7$, where it demonstrates a remarkable 130% enhancement compared to the single-layer SIM. Despite considering practical discrete phase shifts, the proposed SIM only experiences a minor performance loss of less than 0.5 bps as compared to the case with continuous phase shifts. The performance gap can be further narrowed by increasing the value of b . Furthermore, the proposed algorithms outperform all benchmark schemes that consider discrete phase shifts. The quantization method initially exhibits a moderate performance erosion for a small number of metasurface layers, but it degrades significantly as $L > 4$ due to the quantization errors. The average power allocation solution suffers from a performance gap of 1.5 bps in comparison to the iterative water-filling counterpart. Finally, the random phase shift fails to provide any noticeable performance gain as the number of metasurface layers increases.

Fig. 3b depicts the sum rate R versus the number of meta-atoms N on each metasurface layer, using the same system parameters as in Fig. 3a. It is evident that all benchmark schemes attain a performance improvement as N increases. Note that the SIM employing discrete phase shifts with $b = 2$ exhibits a rate penalty of only 0.3 bps compared to its continuous counterpart for all considered settings. Furthermore, Fig. 3b reveals that as N increases, the performance gap between the modified iterative water-filling solution and the average power allocation solution gradually diminishes, which is due to the improved SINR resulting from the larger array aperture

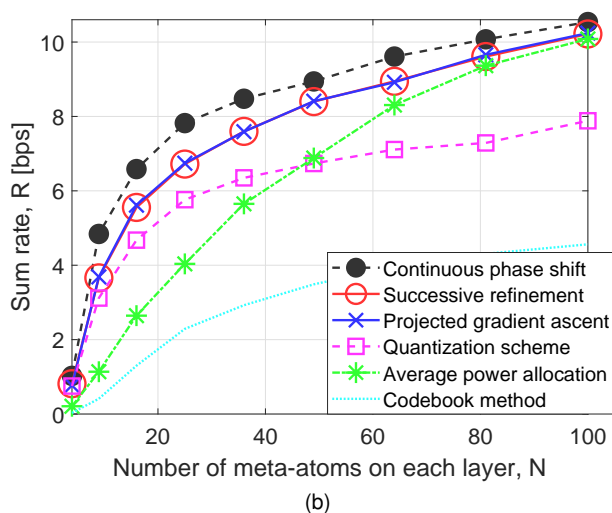
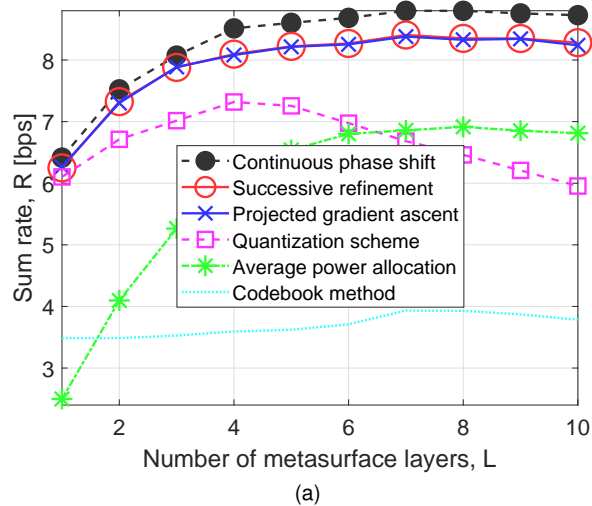


Fig. 3. (a) Sum rate R versus the number of metasurface layers L ; (b) Sum rate R versus the number of meta-atoms N on each metasurface layer.

of SIM. In addition, the proposed successive refinement algorithm consistently outperforms the simple and often utilized quantization scheme, particularly as the number of meta-atoms increases. For example, a significant performance gain of 125% rate increase is attained when $N = 100$. In contrast, the codebook method exhibits only marginal gain as N increases, primarily due to the exponential growth of the searching space for legitimate phase shift vectors with respect to N .

Fig. 4a shows the sum rate versus the number of bits used for quantizing each phase shift, i.e., b , where we set $L = 7$ while keeping the other parameters consistent with Fig. 3a. As expected, the

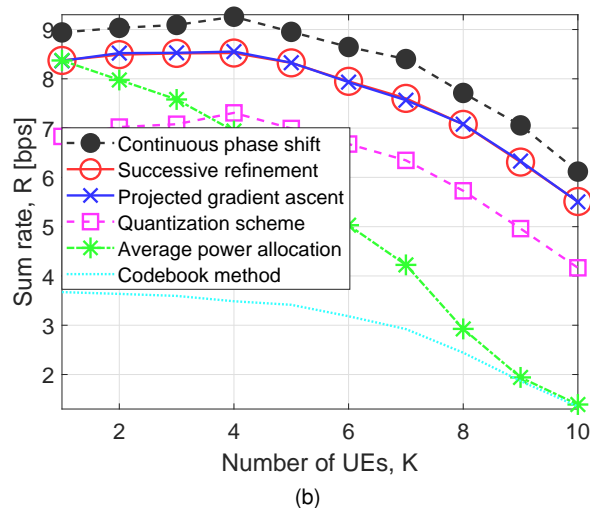
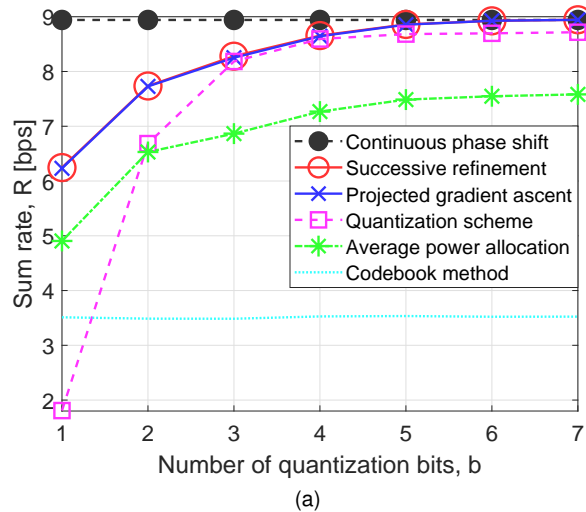
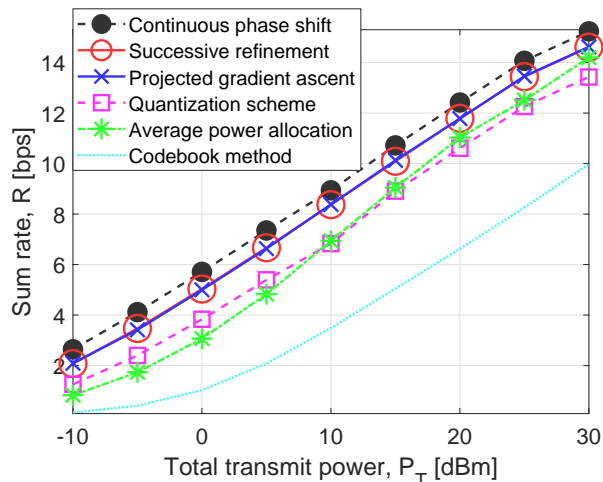


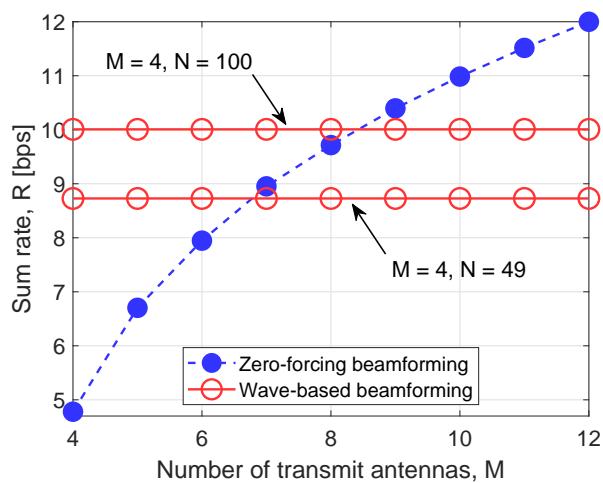
Fig. 4. (a) Sum rate R versus the number of quantization bits b ; (b) Sum rate R versus the number of UEs K .

proposed successive refinement and gradient ascent scheme as well as the quantization method exhibits a gradual improvement in sum rate as b increases, resulting in performance close to that achieved with continuous phase shifts when $b \geq 6$. Specifically, the quantization scheme suffers from a slight rate loss of 0.2 bps. Moreover, the sum rate employing the average power allocation solution also increases with b , but consistently incurs a rate loss of 1.2 bps compared to the iterative water-filling solution. Additionally, the rate performance of the codebook method remains unaffected by the number of quantization bits due to the limited search space.

In Fig. 4b, we plot the achievable sum rate versus the number of UEs K by setting $b = 2$. All



(a)



(b)

Fig. 5. (a) Sum rate R versus the transmit power P_T ; (b) Sum rate comparison of the wave-based beamforming and the conventional ZF beamforming.

the other parameters remain the same as those in Fig. 4a. Note that as K grows, the sum rate with optimized power allocation and wave-based beamforming increases with K at the beginning but decreases when K exceeds a certain threshold. This is due to the fact that the sum rate of a SIM-assisted multiuser MISO system depends on two factors: the *spatial multiplexing gain* brought by an increased number of UEs as well as the *residual interference level* after applying wave-based beamforming. For a large number of UEs, it is more challenging for the SIM to mitigate the inter-user interference. As a result, the sum rate would decrease when the number of UEs exceeds a certain value. In our specific setup with $L = 7$ and $N = 49$, the maximum

number of UEs for which the SIM can effectively mitigate the multiuser interference is $K = 4$. Increasing the number of meta-atoms N could potentially support a greater number of UEs. Furthermore, the quantization method results in a 1.5 bps rate loss under all setups considered in Fig. 4b, while the average power allocation and codebook method fail to adequately suppress the multiuser interference, resulting in performance degradation as the number of UEs increases. For example, the iterative water-filling algorithm achieves a remarkable 400% rate improvement over the average benchmark scheme when the number of UEs is $K = 10$.

Fig. 5a illustrates the sum rate of various schemes versus the transmit power P_T by setting $K = 4$. As expected, the sum rate of all benchmark schemes improves as the transmit power P_T increases. In addition, the proposed successive refinement and projected gradient ascent algorithm outperform both the quantization and codebook methods, exhibiting almost identical performance to continuous phase shifts. Notably, the superiority of the proposed algorithm over the codebook method becomes more pronounced as the transmit power increases, resulting in a rate improvement of 4.5 bps in the moderate and high transmit power regions. Moreover, in the lower power region, the average power allocation suffers from performance erosion as compared to the modified iterative water-filling algorithm. The performance gap, however, becomes negligible as the transmit power grows, which is due to the fact that the water-filling lever is much lower than the power allocated for each UE, rendering the impact of the power allocation negligible.

In Fig. 5b, we compare the sum rate of the SIM-assisted multiuser MISO system and its conventional counterpart without a SIM. In the conventional multiuser MISO downlink system, we employ the classic zero-forcing (ZF) beamforming technique to eliminate multiuser interference. To ensure a fair comparison, we use $d_k = \sqrt{H_{BS}^2 + [d_{UE}(k-1)]^2}$ to characterize the path loss associated with each UE. The power allocation among K UEs is completed by applying the classic water-filling algorithm [11]. Note that the conventional MISO system requires $M = 7$ transmit antenna to outperform the SIM-assisted counterpart with $M = 4$ antennas when considering $N = 49$. When considering the same number of transmit antennas, e.g., $M = 4$, the SIM-assisted system achieves about 200% sum rate improvement compared to conventional MISO systems. Again, thanks to the wave-based beamforming in the SIM, the

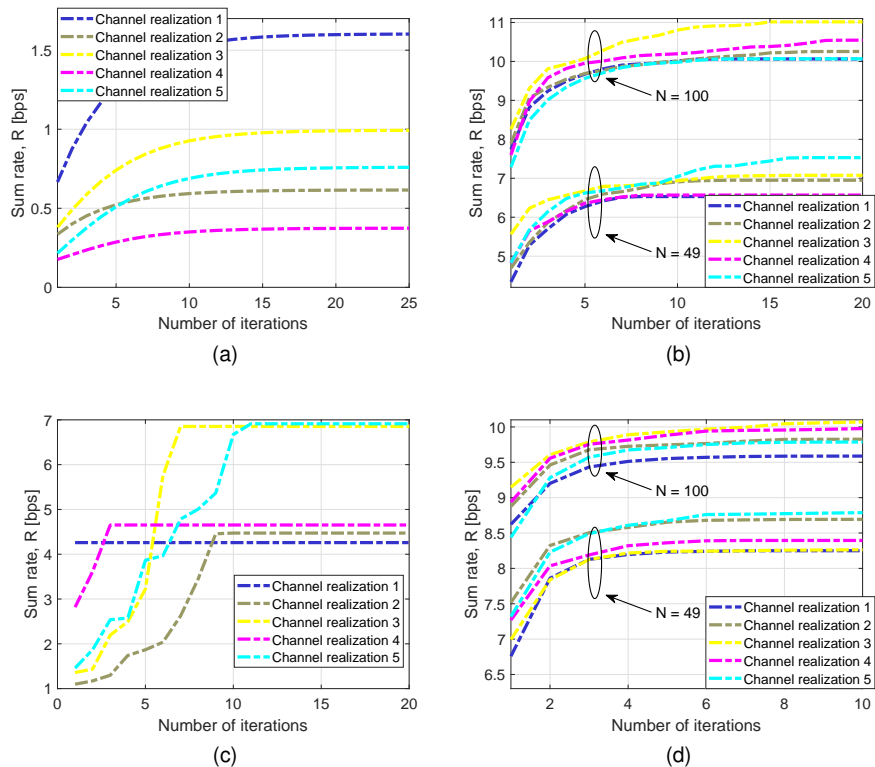


Fig. 6. Convergence behavior of: (a) The iterative water-filling algorithm; (b) The successive refinement algorithm; (c) The projected gradient ascent algorithm; (d) The alternating optimization algorithm.

digital precoding is completely removed at the BS, and each antenna is equipped only with low-resolution ADCs/DACs, which substantially reduces the hardware cost and energy consumption.

C. Convergence of the Proposed Algorithms

Next, we verify the convergence of the proposed algorithms in Section III-B. In Fig. 6a, we show the convergence behavior of the modified iterative water-filling algorithms, while keeping the transmit power fixed at $P_T = 10$ dBm. We consider five independent channel realizations and set random phase shifts for each case. Although the sum rate varies significantly due to the random phase shift, we observe that under all cases the iterative water-filling would converge to its maximum as the iterations progress, which is consistent with the theoretical analysis in [48]. Furthermore, the modified iterative water-filling achieves its maximum within 20 iterations, indicating that $I_{IWF} \leq 20$ in terms of the computational complexity in Section III-C.

Furthermore, we demonstrate the convergence behavior of the proposed successive refinement algorithm and the projected gradient ascent method, taking into account the average power allocation. Fig. 6b presents the rapid convergence of the successive refinement algorithm for two cases: $N = 49$ and $N = 100$. In both setups, the univariate optimization guarantees that the objective function value is non-decreasing and converges within $I_{\text{SR}} \leq 17$ iterations. Nonetheless, at each iteration, the larger number of meta-atoms requires optimizing more phase shifts, resulting in increased complexity.

Moreover, we analyze the convergence behavior of the projected gradient ascent algorithm in Fig. 6c, where we set $N = 49$. It is observed that the projected gradient ascent method converges more rapidly compared to the successive refinement method. Note that we have $I_{\text{GA}} \leq 10$ under the consider setups. Nevertheless, due to the discrete phase shift constraint, the quantitation process at each iteration may bring the algorithm to a local optimum. Thus, under some cases the resultant sum rate in Fig. 6c is slightly lower than that in Fig. 6b, which can be improved by employing multiple sets of initial phase shifts.

In Fig. 6d, we show the convergence of the alternating optimization algorithm, considering two cases of $N = 49$ and $N = 100$. In each case, we examine 10 independent channel realizations. Notably, the outer loop of the alternating optimization algorithm converges very fast, reaching its maximum within 7 iterations under all setups. Therefore, we have $I_{\text{AO}} \leq 7$ in terms of complexity evaluation. Additionally, we observe that increasing the number of meta-atoms leads to a greater number of iterations required for convergence, which is due to the larger amount of optimization variables and the expanded search space.

V. CONCLUSIONS

In this paper, we have proposed a novel SIM design that enables wave-based beamforming in the downlink of a multiuser MISO system. A joint transmit power allocation and phase shift optimization problem was formulated to maximize the sum rate, subject to the transmit power budget and discrete phase shift constraints. To tackle this problem, an alternating optimization algorithm was developed to decompose it into two subproblems. The power allocation was solved by applying a modified iterative water-filling algorithm, while the phase shifts of SIM

were optimized through the projected gradient ascent algorithm and the successive refinement algorithm. Furthermore, we provided insights into the potential benefits of SIM-based operation compared to conventional digital beamforming. Extensive simulation results demonstrated that the proposed joint optimization schemes achieve significant performance gains compared to existing benchmarks.

Finally, our major conclusions are summarized as follows. *First*, increasing the number of metasurface layers can lead to an increase in the sum rate, thanks to the interference cancellation ability of the SIM. Simulation results demonstrated a SIM performing best with seven layers. *Second*, when the number of quantizing bits is greater than four, the performance of a SIM with discretely tuned meta-atoms is almost identical to the continuous counterpart. *Third*, compared to conventional MISO systems, the SIM-based system provided a 200% increase in the sum rate. In a nutshell, SIM devices represent a paradigm shift from conventional digital signal processing to wave-based computation, paving the way for the evolution of energy-efficient wireless networks in the future.

APPENDIX A

PROOF OF PROPOSITION 1

First, we note that the gradient of R with respect to θ_n^l can be expressed as

$$\frac{\partial R}{\partial \theta_n^l} = \log_2 e \sum_{k=1}^K \frac{1}{1 + \gamma_k} \frac{\partial \gamma_k}{\partial \theta_n^l}, \quad \forall n \in \mathcal{N}, \quad \forall l \in \mathcal{L}. \quad (28)$$

Based on the standard quotient rule derivative, $\frac{\partial \gamma_k}{\partial \theta_n^l}$, $\forall k \in \mathcal{K}$ in (28) is given by

$$\begin{aligned} \frac{\partial \gamma_k}{\partial \theta_n^l} &= \frac{p_k}{\sum_{k' \neq k}^K |\mathbf{h}_k^H \mathbf{G} \mathbf{w}_{k'}^1|^2 p_{k'} + \sigma_k^2} \frac{\partial |\mathbf{h}_k^H \mathbf{G} \mathbf{w}_k^1|^2}{\partial \theta_n^l} \\ &\quad - \frac{|\mathbf{h}_k^H \mathbf{G} \mathbf{w}_k^1|^2 p_k}{\left(\sum_{k' \neq k}^K |\mathbf{h}_k^H \mathbf{G} \mathbf{w}_{k'}^1|^2 p_{k'} + \sigma_k^2 \right)^2} \sum_{k' \neq k}^K p_{k'} \frac{\partial |\mathbf{h}_k^H \mathbf{G} \mathbf{w}_{k'}^1|^2}{\partial \theta_n^l}. \end{aligned} \quad (29)$$

By utilizing (29), the partial derivative $\frac{\partial R}{\partial \theta_n^l}$ in (28) can be further simplified to

$$\frac{\partial R}{\partial \theta_n^l} = \log_2 e \sum_{k=1}^K \delta_k \times \left(p_k \frac{\partial |\mathbf{h}_k^H \mathbf{G} \mathbf{w}_k^1|^2}{\partial \theta_n^l} - \gamma_k \sum_{k' \neq k}^K p_{k'} \frac{\partial |\mathbf{h}_k^H \mathbf{G} \mathbf{w}_{k'}^1|^2}{\partial \theta_n^l} \right), \quad (30)$$

where δ_k is defined in (19).

The key challenge in (30) lies in determining the partial derivative of $|\mathbf{h}_k^H \mathbf{G} \mathbf{w}_{k'}^1|^2$ with respect to θ_n^l . Note that $\mathbf{h}_k^H \mathbf{G} \mathbf{w}_{k'}^1$ is linear with respect to $e^{j\theta_n^l}$. Therefore, for any given pair of $(k, k') \in \mathcal{K}^2$, we have

$$\begin{aligned} \frac{\partial |\mathbf{h}_k^H \mathbf{G} \mathbf{w}_{k'}^1|^2}{\partial \theta_n^l} &= \frac{\partial \left| \sum_{n=1}^N e^{j\theta_n^l} \mathbf{h}_k^H \mathbf{v}_n^l (\mathbf{u}_n^l)^H \mathbf{w}_{k'}^1 \right|^2}{\partial \theta_n^l} \\ &= \frac{\partial \Re \left[\left(e^{j\theta_n^l} \mathbf{h}_k^H \mathbf{v}_n^l (\mathbf{u}_n^l)^H \mathbf{w}_{k'}^1 \right) (\mathbf{h}_k^H \mathbf{G} \mathbf{w}_{k'}^1)^H \right]}{\partial \theta_n^l} \\ &= \Im \left[\left(e^{j\theta_n^l} \mathbf{h}_k^H \mathbf{v}_n^l (\mathbf{u}_n^l)^H \mathbf{w}_{k'}^1 \right)^H (\mathbf{h}_k^H \mathbf{G} \mathbf{w}_{k'}^1) \right] \\ &= \eta_{n,k,k'}^l, \end{aligned} \quad (31)$$

where $\eta_{n,k,k'}^l$, $(\mathbf{u}_n^l)^H$, and \mathbf{v}_n^l are defined in (20), (21), and (22), respectively.

Upon substituting (31) into (30), the proof is completed. ■

REFERENCES

- [1] J. An, M. Di Renzo, M. Debbah, and C. Yuen, "Stacked intelligent metasurfaces for multiuser beamforming in the wave domain," in *Proc. IEEE Int. Conf. Commun. (ICC)*, Rome, Italy, May 2023, pp. 1–6.
- [2] F. Boccardi, R. W. Heath, A. Lozano, T. L. Marzetta, and P. Popovski, "Five disruptive technology directions for 5G," *IEEE Commun. Mag.*, vol. 52, no. 2, pp. 74–80, Feb. 2014.
- [3] F. S. S. and W. Yu, "Hybrid digital and analog beamforming design for large-scale antenna arrays," *IEEE J. Sel. Topics Signal Process.*, vol. 10, no. 3, pp. 501–513, Apr. 2016.
- [4] T. S. Rappaport, G. R. MacCartney, M. K. Samimi, and S. Sun, "Wideband millimeter-wave propagation measurements and channel models for future wireless communication system design," *IEEE Trans. Commun.*, vol. 63, no. 9, pp. 3029–3056, Sep. 2015.

- [5] J. An, C. Xu, L. Wang, Y. Liu, L. Gan, and L. Hanzo, "Joint training of the superimposed direct and reflected links in reconfigurable intelligent surface assisted multiuser communications," *IEEE Trans. Green Commun. Netw.*, vol. 6, no. 2, pp. 739–754, Jun. 2022.
- [6] J. Zhang, E. Björnson, M. Matthaiou, D. W. K. Ng, H. Yang, and D. J. Love, "Prospective multiple antenna technologies for beyond 5G," *IEEE J. Sel. Areas Commun.*, vol. 38, no. 8, pp. 1637–1660, Aug. 2020.
- [7] J. An, H. Li, D. W. K. Ng, and C. Yuen, "Fundamental detection probability vs. achievable rate tradeoff in integrated sensing and communication systems," *IEEE Trans. Wireless Commun.*, pp. 1–19, 2023, Early Access.
- [8] M. Di Renzo, A. Zappone, M. Debbah, M.-S. Alouini, C. Yuen, J. de Rosny, and S. Tretyakov, "Smart radio environments empowered by reconfigurable intelligent surfaces: How it works, state of research, and the road ahead," *IEEE J. Sel. Areas Commun.*, vol. 38, no. 11, pp. 2450–2525, Nov. 2020.
- [9] Y. Liu, X. Liu, X. Mu, T. Hou, J. Xu, M. Di Renzo, and N. Al-Dhahir, "Reconfigurable intelligent surfaces: Principles and opportunities," *IEEE Commun. Surveys Tuts.*, vol. 23, no. 3, pp. 1546–1577, 3rd Quart. 2021.
- [10] C. Huang, A. Zappone, G. C. Alexandropoulos, M. Debbah, and C. Yuen, "Reconfigurable intelligent surfaces for energy efficiency in wireless communication," *IEEE Trans. Wireless Commun.*, vol. 18, no. 8, pp. 4157–4170, Aug. 2019.
- [11] J. An, C. Xu, L. Gan, and L. Hanzo, "Low-complexity channel estimation and passive beamforming for RIS-assisted MIMO systems relying on discrete phase shifts," *IEEE Trans. Commun.*, vol. 70, no. 2, pp. 1245–1260, Feb. 2022.
- [12] Z. Wan, Z. Gao, F. Gao, M. D. Renzo, and M.-S. Alouini, "Terahertz massive MIMO with holographic reconfigurable intelligent surfaces," *IEEE Trans. Commun.*, vol. 69, no. 7, pp. 4732–4750, Jul. 2021.
- [13] C. Xu, J. An, T. Bai, S. Sugiura, R. G. Maunder, Z. Wang, L.-L. Yang, and L. Hanzo, "Channel estimation for reconfigurable intelligent surface assisted high-mobility wireless systems," *IEEE Trans. Veh. Technol.*, vol. 72, no. 1, pp. 718–734, Jan. 2023.
- [14] Q. Wu, S. Zhang, B. Zheng, C. You, and R. Zhang, "Intelligent reflecting surface-aided wireless communications: A tutorial," *IEEE Trans. Commun.*, vol. 69, no. 5, pp. 3313–3351, May 2021.
- [15] C. Pan, G. Zhou, K. Zhi, S. Hong, T. Wu, Y. Pan, H. Ren, M. Di Renzo, A. Lee Swindlehurst, R. Zhang, and A. Y. Zhang, "An overview of signal processing techniques for RIS/IRS-aided wireless systems," *IEEE J. Sel. Topics Signal Process.*, vol. 16, no. 5, pp. 883–917, Aug. 2022.
- [16] J. An, Q. Wu, and C. Yuen, "Scalable channel estimation and reflection optimization for reconfigurable intelligent surface-enhanced OFDM systems," *IEEE Wireless Commun. Lett.*, vol. 11, no. 4, pp. 796–800, Apr. 2022.
- [17] Q.-U.-A. Nadeem, A. Kammoun, A. Chaaban, M. Debbah, and M.-S. Alouini, "Asymptotic max-min SINR analysis of reconfigurable intelligent surface assisted MISO systems," *IEEE Trans. Wireless Commun.*, vol. 19, no. 12, pp. 7748–7764, Dec. 2020.
- [18] Q. Wu and R. Zhang, "Beamforming optimization for wireless network aided by intelligent reflecting surface with discrete phase shifts," *IEEE Trans. Commun.*, vol. 68, no. 3, pp. 1838–1851, Mar. 2020.
- [19] J. An and L. Gan, "The low-complexity design and optimal training overhead for IRS-assisted MISO systems," *IEEE Wireless Commun. Lett.*, vol. 10, no. 8, pp. 1820–1824, Aug. 2021.
- [20] W. Tang, X. Chen, M. Z. Chen, J. Y. Dai, Y. Han, M. Di Renzo, S. Jin, Q. Cheng, and T. J. Cui, "Path loss modeling and measurements for reconfigurable intelligent surfaces in the millimeter-wave frequency band," *IEEE Trans. Commun.*, vol. 70, no. 9, pp. 6259–6276, Sep. 2022.

- [21] J. An, C. Xu, Q. Wu, D. W. K. Ng, M. Di Renzo, C. Yuen, and L. Hanzo, "Codebook-based solutions for reconfigurable intelligent surfaces and their open challenges," *IEEE Wireless Commun.*, pp. 1–8, 2023, Early Access.
- [22] B. Di, H. Zhang, L. Song, Y. Li, Z. Han, and H. V. Poor, "Hybrid beamforming for reconfigurable intelligent surface based multi-user communications: Achievable rates with limited discrete phase shifts," *IEEE J. Sel. Areas Commun.*, vol. 38, no. 8, pp. 1809–1822, Aug. 2020.
- [23] W. Xu, J. An, Y. Xu, C. Huang, L. Gan, and C. Yuen, "Time-varying channel prediction for RIS-assisted MU-MISO networks via deep learning," *IEEE Trans. Cognitive Commun. Netw.*, vol. 8, no. 4, pp. 1802–1815, Dec. 2022.
- [24] X. Yu, D. Xu, Y. Sun, D. W. K. Ng, and R. Schober, "Robust and secure wireless communications via intelligent reflecting surfaces," *IEEE J. Sel. Areas Commun.*, vol. 38, no. 11, pp. 2637–2652, Nov. 2020.
- [25] C. Xu, J. An, T. Bai, L. Xiang, S. Sugiura, R. G. Maunder, L.-L. Yang, and L. Hanzo, "Reconfigurable intelligent surface assisted multi-carrier wireless systems for doubly selective high-mobility Ricean channels," *IEEE Trans. Veh. Technol.*, vol. 71, no. 4, pp. 4023–4041, Apr. 2022.
- [26] H. Guo, Y.-C. Liang, J. Chen, and E. G. Larsson, "Weighted sum-rate maximization for reconfigurable intelligent surface aided wireless networks," *IEEE Trans. Wireless Commun.*, vol. 19, no. 5, pp. 3064–3076, May 2020.
- [27] W. Xu, J. An, C. Huang, L. Gan, and C. Yuen, "Deep reinforcement learning based on location-aware imitation environment for RIS-aided mmwave MIMO systems," *IEEE Wireless Commun. Lett.*, vol. 11, no. 7, pp. 1493–1497, Jul. 2022.
- [28] T. Van Chien, H. Q. Ngo, S. Chatzinotas, M. Di Renzo, and B. Ottersten, "Reconfigurable intelligent surface-assisted cell-free massive MIMO systems over spatially-correlated channels," *IEEE Trans. Wireless Commun.*, vol. 21, no. 7, pp. 5106–5128, Jul. 2022.
- [29] C. Xu, J. An, T. Bai, S. Sugiura, R. G. Maunder, L.-L. Yang, M. Di Renzo, and L. Hanzo, "Antenna selection for reconfigurable intelligent surfaces: A transceiver-agnostic passive beamforming configuration," *IEEE Trans. Wireless Commun.*, pp. 1–18, 2023, Early Access.
- [30] A. Papazafeiropoulos, C. Pan, P. Kourtessis, S. Chatzinotas, and J. M. Senior, "Intelligent reflecting surface-assisted MU-MISO systems with imperfect hardware: Channel estimation and beamforming design," *IEEE Trans. Wireless Commun.*, vol. 21, no. 3, pp. 2077–2092, Mar. 2022.
- [31] X. Jia, J. An, H. Liu, H. Liao, L. Gan, and C. Yuen, "Environment-aware codebook for reconfigurable intelligent surface-aided MISO communications," *IEEE Wireless Commun. Lett.*, pp. 1–5, 2023, Early Access.
- [32] Y. Han, W. Tang, S. Jin, C.-K. Wen, and X. Ma, "Large intelligent surface-assisted wireless communication exploiting statistical CSI," *IEEE Trans. Veh. Technol.*, vol. 68, no. 8, pp. 8238–8242, Aug. 2019.
- [33] W. Xu, J. An, H. Li, L. Gan, and C. Yuen, "Algorithm unrolling-based distributed optimization for RIS-assisted cell-free networks," *IEEE Int. Things J.*, pp. 1–15, 2023, Early Access.
- [34] Q. Spencer, A. Swindlehurst, and M. Haardt, "Zero-forcing methods for downlink spatial multiplexing in multiuser MIMO channels," *IEEE Trans. Signal Process.*, vol. 52, no. 2, pp. 461–471, Feb. 2004.
- [35] J. An, C. Xu, D. W. K. Ng, G. C. Alexandropoulos, C. Huang, C. Yuen, and L. Hanzo, "Stacked intelligent metasurfaces for efficient holographic MIMO communications in 6G," *IEEE J. Sel. Areas Commun.*, vol. 41, no. 8, pp. 2380–2396, Aug. 2023.
- [36] X. Lin, Y. Rivenson, N. T. Yardimci, M. Veli, Y. Luo, M. Jarrahi, and A. Ozcan, "All-optical machine learning using diffractive deep neural networks," *Sci.*, vol. 361, no. 6406, pp. 1004–1008, Jul. 2018.

- [37] C. Liu, Q. Ma, Z. J. Luo, Q. R. Hong, Q. Xiao, H. C. Zhang, L. Miao, W. M. Yu, Q. Cheng, L. Li *et al.*, “A programmable diffractive deep neural network based on a digital-coding metasurface array,” *Nat. Electro.*, vol. 5, no. 2, pp. 113–122, 2022.
- [38] J. Choi, J. Mo, and R. W. Heath, “Near maximum-likelihood detector and channel estimator for uplink multiuser massive MIMO systems with one-bit ADCs,” *IEEE Trans. Commun.*, vol. 64, no. 5, pp. 2005–2018, May 2016.
- [39] J. W. Goodman, *Introduction to Fourier Optics*. Roberts and Company Publishers, 2005.
- [40] J. An, C. Yuen, C. Huang, M. Debbah, H. V. Poor, and L. Hanzo, “A tutorial on holographic MIMO communications—part I: Channel modeling and channel estimation,” *IEEE Commun. Lett.*, pp. 1–5, 2023, Early Access.
- [41] —, “A tutorial on holographic MIMO communications—part II: Performance analysis and holographic beamforming,” *IEEE Commun. Lett.*, vol. 27, no. 7, pp. 1669–1673, Jul. 2023.
- [42] —, “A tutorial on holographic MIMO communications—part III: Open opportunities and challenges,” *IEEE Commun. Lett.*, vol. 27, no. 7, pp. 1674–1678, Jul. 2023.
- [43] E. Björnson and L. Sanguinetti, “Rayleigh fading modeling and channel hardening for reconfigurable intelligent surfaces,” *IEEE Wireless Commun. Lett.*, vol. 10, no. 4, pp. 830–834, Apr. 2021.
- [44] S. Sanayei and A. Nosratinia, “Antenna selection in MIMO systems,” *IEEE Commun. Mag.*, vol. 42, no. 10, pp. 68–73, Oct. 2004.
- [45] A. Molisch and M. Win, “MIMO systems with antenna selection,” *IEEE Microwave Mag.*, vol. 5, no. 1, pp. 46–56, Mar. 2004.
- [46] S. Sugiura and L. Hanzo, “Effects of channel estimation on spatial modulation,” *IEEE Signal Process. Lett.*, vol. 19, no. 12, pp. 805–808, Dec. 2012.
- [47] W. Yu, W. Rhee, S. Boyd, and J. Cioffi, “Iterative water-filling for Gaussian vector multiple-access channels,” *IEEE Trans. Inf. Theory*, vol. 50, no. 1, pp. 145–152, Jan. 2004.
- [48] N. Jindal, W. Rhee, S. Vishwanath, S. Jafar, and A. Goldsmith, “Sum power iterative water-filling for multi-antenna Gaussian broadcast channels,” *IEEE Trans. Inf. Theory*, vol. 51, no. 4, pp. 1570–1580, Apr. 2005.
- [49] D. Tse and P. Viswanath, *Fundamentals of Wireless Communication*. Cambridge university press, 2005.
- [50] L. Armijo, “Minimization of functions having Lipschitz continuous first partial derivatives,” *Pac. J. Math.*, vol. 16, no. 1, pp. 1–3, Jan. 1966.